Acta Materialia 195 (2020) 621–630

Contents lists available at ScienceDirect

Acta Materialia

journal homepage: www.elsevier.com/locate/actamat

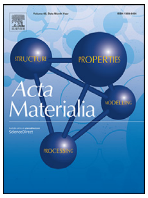

Full length article

Radiation tolerance and microstructural changes of nanocrystalline Cu-Ta alloy to high dose self-ion irradiation

S. Srinivasan[a], C. Kale[a], B.C. Hornbuckle[b], K.A. Darling[b], M.R. Chancey[c], E. Hernández-Rivera[b], Y. Chen[d], T.R. Koenig[e], Y.Q. Wang[c], G.B. Thompson[e], K.N. Solanki[a,*]

[a] School for the Engineering of Matter, Transport, and Energy, Arizona State University, Tempe, AZ, 85287, USA
[b] US CCDC Army Research Laboratory, Weapons, and Materials Research Directorate, APG, MD 21005, USA
[c] Materials Science and Technology Division, Los Alamos National Laboratory, Los Alamos, NM 87545, USA
[d] CAMECA Instruments Inc, 5470 Nobel Drive, Madison WI, 53711, USA
[e] Department of Metallurgical & Materials Engineering, The University of Alabama, Tuscaloosa, AL 35401, USA

ARTICLE INFO

Article history:
Received 2 February 2020
Revised 22 May 2020
Accepted 25 May 2020
Available online 5 June 2020

Keywords:
Nanocrystalline
Irradiation effect
Transmission electron microscopy
Immiscible system
Phase stability

ABSTRACT

Nanocrystalline materials are known to possess excellent radiation resistance due to high fraction of grain boundaries that act as defect sinks, provided they are microstructurally stable at such extreme conditions. In this work, radiation response of a stable nanocrystalline Cu-Ta alloy is studied by irradiating with 4 MeV copper ions to doses (close to the surface) of 1 displacements per atom (dpa) at room temperature (RT); 10 dpa at RT, 573 and 723 K; 100 and 200 dpa at RT and 573 K. Nanoindentation results carried out for samples irradiated till 100 dpa at RT and 573 K show exceptionally low radiation hardening behavior compared to various candidate materials from literature. Results from microstructural characterization, using atom probe analysis and transmission electron microscopy, show a stable nanocrystalline microstructure with minimal grain growth and a meagre swelling in samples irradiated to 100 dpa (~0.2%) and 200 dpa at RT, while no voids in those at 573 K. This radiation tolerance is partly attributed to the stability of Ta nanoclusters due to phase separating nature of the alloy. Additionally, the larger tantalum particles are observed to undergo ballistic dissolution at doses greater than 100 dpa and are eventually precipitated as nanoclusters, replenishing the sink strength, which enhanced material's radiation tolerance when exposed to high irradiation doses and elevated temperatures.

1. Introduction

Increasing concerns about global warming and carbon dioxide (CO_2) emissions have raised the demand for renewable and sustainable energy sources, such as nuclear energy. However, development of advanced structural materials for next generation reactors is challenging due to harsh reactor environment viz. high energy neutron exposure, temperature and corrosion environment [1,2]. Radiation induced displacement cascade generates high density of vacancies and interstitials (Frenkel pairs) which coalesce to form defect clusters like interstitial dislocation loops, voids and stacking fault tetrahedra (SFT), eventually posing serious threats like radiation-hardening and embrittlement, phase instabilities from radiation induced precipitates, irradiation creep, volumetric swelling from void formation, and high temperature helium embrittlement [3].

Interfaces like grain boundaries and phase boundaries act as efficient sinks to annihilate radiation induced defects. Designing materials with large fraction of natural defect sinks is the key to alleviate radiation effects. The current state of the art materials for reactor application are reduced activation ferritic-martensitic (RAFM) and oxide dispersion strengthened (ODS) steels. ODS steels are of great interest due to their superiority in defect sink efficiency and high temperature properties attributed to the fine oxide dispersions [4]. However, they are still not completely immune to radiation hardening at considerably high doses [5,6] and the stability of oxide phases (dissolution, growth and amorphization) are not well understood due to inconsistency with results observed in literature [7]. Various research on other advanced materials such as nano layered composites have shown that improving interface concentration (i.e. reducing the spacing of nano layers) creates overlapping void denuded zones which is the key aspect in achieving void free structure [8–10]. Likewise, nanocrystalline (NC) materials are one of the promising candidates due to high volume fraction of grain boundaries which act as unbiased sinks

---

[*] Corresponding author.
E-mail address: kiran.solanki@asu.edu (K.N. Solanki).

https://doi.org/10.1016/j.actamat.2020.05.061
1359-6454/© 2020 Acta Materialia Inc. Published by Elsevier Ltd. All rights reserved.

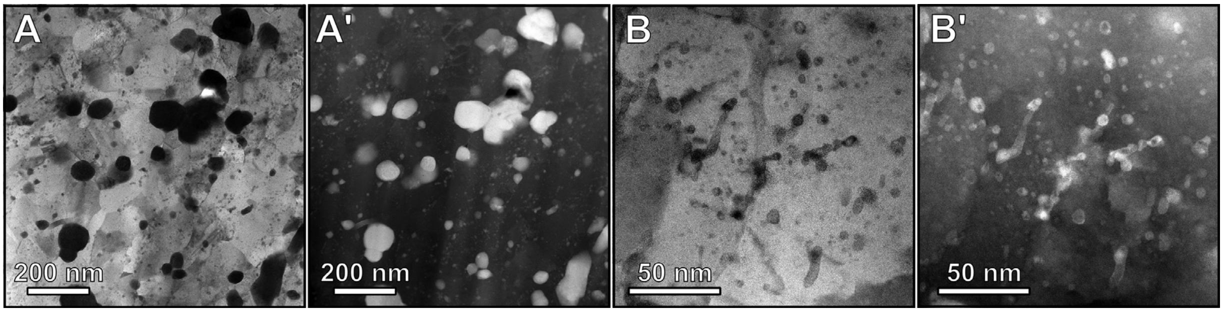

Fig. 1. As-received microstructure. STEM images of unirradiated (A-B) NC Cu-10at. %Ta. (A') and (B') are the corresponding HAADF image to the bright field STEM images in (A) and (B) respectively.

for radiation defects [11,12]. However, microstructural instabilities (e.g., grain growth) observed during high energy neutron radiation complicate the interpretation of grain size effects [13]; reduces the sink concentration and efficiency, leading to a reduction in performance and lifetime [14]. Thus, the hunt continues for materials that prolong the life cycle of nuclear reactors, i.e., not only immune to radiation induced degradation but also maintain/enhance their mechanical properties during sustained radiation exposure.

The core strategy of this work is to maintain stable length scale or microstructural unit along with the presence of a sacrificial phase in an immiscible alloy system for enhanced radiation tolerance. Immiscible alloys driven far from equilibrium through mechanical alloying or irradiation, such as Cu-Ta, Cu-Nb, Cu-V, Cu-Mo, Ni-Ag, Ag-Fe, Ag-Cu etc., have been of great interest to researchers, since their response to severe plastic deformation/radiation is unique compared to their miscible counterparts (or those with low heat of mixing), due to the competition between ballistic mixing and thermodynamically driven kinetics such as decomposition and phase separation [15–17]. Here, we use NC Cu-10 at. % Ta alloy (referred to herein as NC Cu-Ta alloy) with Ta nanoclusters of average diameter 3 nm and a spatial arrangement of proportional length scale, as a model material system. Recent works on this alloy have shown that introduction of stable nano dispersions led to extraordinary strength, thermomechanical stability and creep properties [18,19], along with high thermal and electrical conductivity [20]. Combining these unique mechanical, thermal and electrical properties with radiation tolerance will open avenues for applications such as high temperature heat exchanger and other reactor components. In this study, we primarily focused on investigating NC Cu-Ta alloy's self-ion irradiation response related to three of the most detrimental radiation effects, i.e., radiation induced hardening, void swelling, and microstructural/phase instability to elucidate the radiation tolerance behavior of a stable nanocrystalline material.

2. Material and methodology

2.1. Processing and as-received microstructure

The material was produced by high energy ball milling followed by equal channel angular extrusion, refer [18]. As-received microstructural characterization (Fig. 1) using transmission electron microscopy (TEM) revealed the presence of Cu grains with an average size of 50 ± 18 nm as well as Ta particles. Processing produced a wide range of Ta particle sizes, ranging from atomic nanoclusters ($\leq$ 15 nm) of average diameter 3.18 ± 0.86 nm to much larger sacrificial precipitates ($>$15 nm) of average diameter 32 ± 8 nm [21]. Previous works had indicated that this material has coherent, semi-coherent, and incoherent Ta precipitates (diameters of $<$3.9 nm, 3.9–15.6 nm and $>$15. nm, respectively) [18]. Further, the Ta nanoclusters also have misfit lattice dislocations at the interface with an average misfit strain of about 5.8%, but can be as high as 11% [18,21,22].

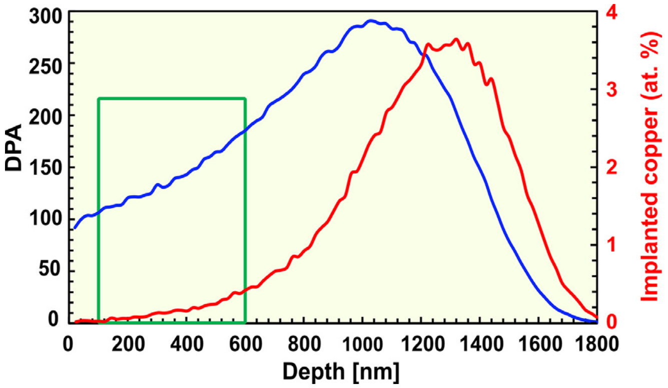

Fig. 2. SRIM Damage profile. Dpa profile and implanted Cu in at. % for NC Cu-10at. %Ta irradiated with 4 MeV Cu^{++} ions to a fluence of 2 × 10^{17} ions cm^{-2}

2.2. Irradiation experiments and SRIM analysis

NC Cu-Ta cylindrical specimens with 3 mm diameter and ~1.2 mm tall, were mechanically polished to a mirror finish and irradiated with a defocused beam of 4 MeV Cu^{++} ions. A flux of ~9 × 10^{12} ions cm^{-2} s^{-1} was used to achieve fluences of 2 × 10^{15} ions cm^{-2} at room temperature (RT); 2 × 10^{16} ions cm^{-2} at RT, 573, and 723 K; 2 × 10^{17} and 4 × 10^{17} ions cm^{-2} at RT and 573 K. The samples were mounted to the heating stage with silver paste for good thermal conduction and the stage temperature was monitored through a thermocouple attached to the stage. Damage profiles were calculated using Stopping and Range of Ions in Matter (SRIM) software utilizing the Kinchin Pease model, which gives the best correlation with the internationally adopted Norgett, Robinson, and Torrens (NRT) displacement model [23]. The simulation was performed for Cu-10at.%Ta with threshold displacement energy of copper and tantalum set to 30 eV and 90 eV respectively [24]. Damage profiles in displacements per atom (dpa, Fig. 2), indicate a damage level of 100 dpa near the surface (relatively flat) for the fluence 2 × 10^{17} ions cm^{-2}, with peak damage occurring at ~1.1 µm. Similarly, other fluences had a dpa of 1, 10 and 200 dpa at the surface respectively (Fig. S1). Henceforth, nomenclature for the irradiated samples will correspond to the flat damage region on the surface, i.e. 1 dpa, 10 dpa, 100 dpa and 200 dpa. Approximate dose rates near the surface and peak damage were calculated to be 0.0045 and 0.015 dpa/s respectively. The depth range highlighted in green (away from the peak damage where the dose rate variation is relatively minimum) was utilized for analyzing the grain and void statistics.

2.3. Nanoindentation experiments

Displacement controlled nanoindentation was carried out using TI 980 TriboIndenter with a Berkovich diamond tip of radius 150 nm. Indentation depth was fixed at 200 nm to maintain a balance between the effect of plastic zone probing past the peak zone into the unirradiated region at higher depths and indentation size effects and surface effects at lower depth [25]. A three segment quasi-static loading profile with load and unload period of 10.6 s and hold period of 7 s was utilized. More than 25 indents were used for every condition to get good statistical information. Each indent was spaced 10 µm apart to avoid overlap of their radial plastic zones. The surface was mechanically polished to mirror finish till 0.05 µm colloidal silica suspension. Surface finish post irradiation was not affected significantly due to sputtering till 100 dpa. Maximum Standard deviation for the indentation hardness was 7.5% indicating statistically precise measurements. However, at 200 dpa, the irradiated surface had high roughness due to sputtering, and hence nanoindentation could not be carried out.

2.4. Grazing Incidence X-ray Diffraction experiments

PANalytical Xpert Pro with Cu kα radiation source was utilized to get Grazing Incidence X-Ray Diffraction patterns. Mirrors and parallel plate collimators were utilized for incident beam and diffracted beam optics respectively. Scans were carried out at an omega of 2° which gives an attenuation depth of nearly 750 nm in copper which is well within the irradiated depth. A step size of 0.0125° with a time per step of 0.2 s was utilized for the scans. Peak positions and intensity of Cu and Ta were analyzed to get some insight on lattice distortion and phase stability post irradiation.

2.5. Microstructural characterization

For transmission electron microscopy (TEM) characterizations carried out in ARM-200F, samples were prepared using a Focused Ion beam (FIB) FEI Nova 500 to get cross section liftouts of the irradiated region which were thinned to electron transparency till 2 keV and were plasma cleaned in Ar prior to TEM observations to reduce contamination. EDS and EELS were performed with a step size of 1 nm and a dwell time of 0.1 s. Grain size and void statistics were obtained from depths spanning 100–600 nm from the irradiated surface to minimize the effects of surface and interstitials in peak damage region. More than 150 grains were sampled for each irradiation condition using ImageJ software to get the average grain size. Nanoclusters and voids statistics were determined with the help of HAADF (High Annular Angular Dark Field) images. Under and over focused TEM BF images were utilized to confirm small voids, which were difficult to detect. Swelling analysis was done by quantifying voids size and density using Image J software and averaging over 2-3 liftouts for each condition. Swelling percentage was calculated as given below [26],

$$\text{Swelling } (\%) = 100\,\frac{\text{Volume of voids}}{\text{Volume of lamella without voids}} = 100\,\frac{\frac{\pi}{6}\sum_{i=1}^{N} {d_i}^3}{A.t - \frac{\pi}{6}\sum_{i=1}^{N} {d_i}^3} \quad (1)$$

where d is the void diameter, N is the total number of voids, A is the area of the lamella investigated and t is the thickness of the lamella.

2.6. Sink strength calculations

Sink strengths of GBs of grain size h and the nanoclusters of diameter D and number density N were calculated based on the equations (2) given below [27],

$$S_b = \frac{15}{h^2} \text{ and } S_{ppt} = 2\pi ND \quad (2)$$

2.7. Atom probe tomography

APT was performed using a CAMECA Local Electrode Atom Probe (LEAP) 5000 XS instrument. The specimens irradiated to 100 dpa at RT and 573 K were lifted-out from the irradiated surface and welded to a pre-fabricated Si post using a Thermofisher Helios 660 dual-beam scanning electron microscope and focused ion beam (SEM/FIB) with a Ga source equipped with an EasyLift Nanomanipulator system. Specimens were then sharpened to a needle-shape geometry with a final tip diameter of 100 nm using annular ion beam milling at 30kV, followed by 1 kV cleaning. The field evaporation was performed at 30 K with a laser pulse energy of 50 pJ, auto pulse control limit of 300 Da and a target evaporation rate of 0.5 %. Clustering was evaluated through the cluster analysis functions in Integrated Visualization and Analysis Software (IVAS) utilizing the maximum separation algorithm as determined in [28].

3. Results and discussion

3.1. Radiation hardening

Radiation hardening is one of the major issues responsible for embrittlement of structural reactor components. Thus, to study radiation hardening behavior of NC Cu-Ta alloy, displacement-controlled nano-indentation experiments were performed on the irradiated surface (Experimental Section). Indentations were carried out at a depth of 200 nm, where the dpa profile is relatively flat. However, the measured hardness values correspond to a larger volume that spans a range of radiation doses higher than that for which they are reported, due to extension of the plastic zone generated from the indentation [29]. Post irradiation hardness data for NC Cu-Ta is plotted in supplementary Fig. S2. Fig. 3 shows the change in hardness at 298 K and at 573 K for various irradiated alloys in comparison with NC Cu-Ta alloy. Note that for literature data, the values for change in hardness have been obtained either through direct measurements such as nano-indentation/micro-indentation or indirect measurements such as tensile yield strength converted into hardness. In the case of radiation hardening at 298 K, (Fig. 3A), the percentage change in hardness from as-received (0 dpa) to 1 and 10 dpa in NC Cu-Ta alloy is negligible. On the contrary, for similar dpa levels, the radiation hardening for coarse-grained pure Cu is about ~80% (24% at a very low dose of 0.034 dpa) [30] and that for some nano-layered composites is about ~15% [31]. Furthermore, at 100 dpa, NC Cu-Ta shows a hardening of mere ~15%, which is similar to the amount of radiation hardening observed in other materials at 1-2 dpa (Fig. 3A). Hence, it can be inferred that NC Cu-Ta alloy has high-level of tolerance to radiation hardening at 298 K. Likewise, hardening comparison at 573 K, Fig. 3B, shows some of the notable materials, the ferritic ODS steels and ferritic martensitic steels, experiencing a steep increase in hardness post-radiation at low to moderate damage levels. For instance, MA 957 shows a hardening of 7% at 6.5 dpa and 48% at 42 dpa [5,32]. However, NC Cu-Ta alloy exhibits a minimal hardening of 0.4% and 5.5% at dose levels of 10 and 100 dpa, respectively at 573 K. Overall, it is evident that NC Cu-Ta alloy retains its hardness up to considerably high dose levels reached in generation IV reactors, indicating exceptional resistance to radiation hardening.

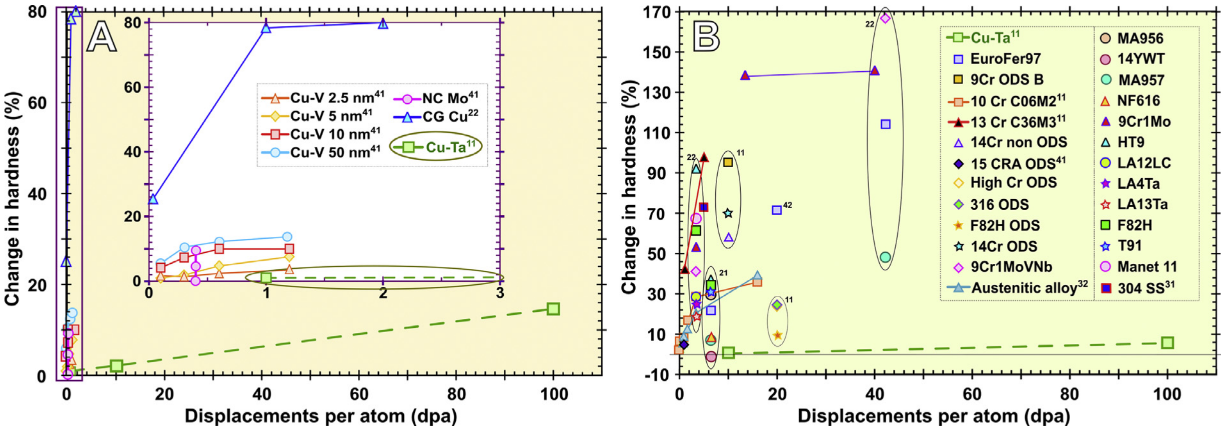

Fig. 3. Percentage irradiation hardening for NC Cu-Ta and various materials from literature, at different doses irradiated at (A) 298 K and (B) 573 K [5,6,11,30–39]. Note that numbers in the super scripts (on legends and data points) represent irradiation ion type, and testing method carried out for calculating hardening respectively; where 1- Heavy/self-ion, 2- neutron, 3-proton and 4-helium ion, in the first letter of superscript and 1- Indentation and 2- Tension test, in the second letter of superscript.

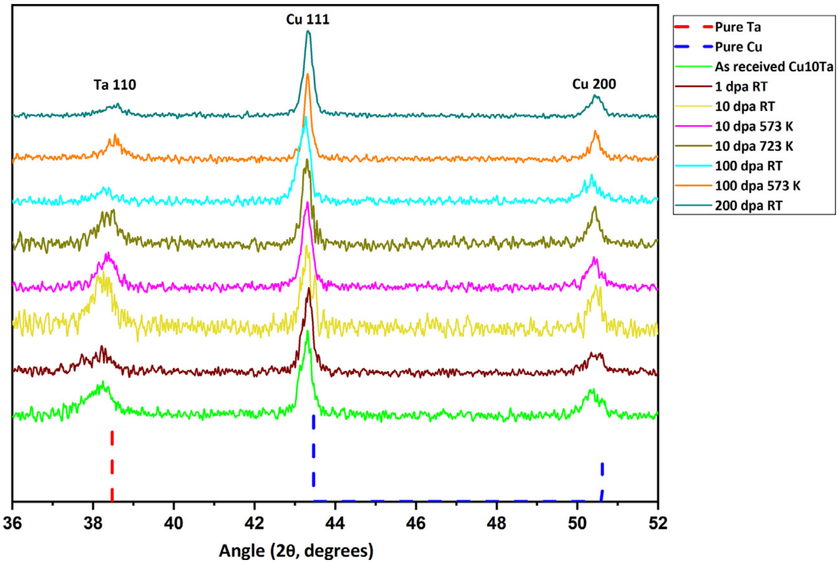

Fig. 4. Grazing Incidence XRD characterization. Grazing incidence X-ray Diffraction data for NC Cu-Ta irradiated at various conditions, indicating negligible lattice distortion. The peak positions generated for pure Cu and Ta for comparison, were taken from the ICDD database.

3.2. Lattice stability

Radiation exposure is also known to cause lattice and phase instabilities leading to lattice distortion and disordering. Grazing incidence X-ray diffraction (GIXD) studies on NC Cu-Ta show a minimum lattice parameter change for all irradiation conditions (Fig. 4 and Table S1). Lattice contraction of ~0.7% (negligible considering experimental uncertainty) observed in Ta peaks at 200 dpa may be attributed to strain relaxation (processing induced). A similar structural contraction of ~1.42% was observed in NC ZrN upon increasing the dose to 5 dpa after which the lattice contraction saturated [40]. Additionally, high concentration of implanted Cu in the Ta precipitates at higher dose, could have also caused this contraction in Ta peak since the atomic radius of Cu is smaller than Ta. Further, XRD and TEM studies of helium ion irradiated Cu-V 2.5 nm multilayers in literature had shown a peak lattice expansion of 1.2% at 5 dpa [31,41]. However, in NC Cu-Ta alloy, no significant distortion of copper lattice was observed up to a dose of 200 dpa. Further, a slight drop in Ta peak intensity relative to Cu, observed at higher doses (100 dpa and beyond) could be attributed to amorphization or dissolution of larger Ta particles. However, since no significant lattice expansion was observed in Cu peaks post irradiation (as expansion could indicate Ta entering Cu lattice as solid solution, as observed in as-milled Cu-Ta post mechanical alloying [42]), significant portion of dissolved Ta could be distributed as fine precipitates. An important takeaway from these results is that there is a minimal change in lattice parameter of Cu or Ta at very high doses, indicating the lattice stability of NC Cu-Ta system at very high dpa levels.

3.3. Post irradiation microstructure

3.3.1. Microstructural stability and void swelling

To understand the extraordinary resistance to radiation hardening and lattice stability of NC Cu-Ta alloy, we drive our attention to post irradiation microstructural analysis at various damage conditions. Fig. 5 shows low and high magnification bright field STEM images of NC Cu-Ta alloy tested at different fluences at RT and 573 K, revealing several significant features. As observed in the Fig. 5A-B, microstructure of NC Cu-Ta alloy at 10 dpa showed a small increase in the average grain size from 50 nm in as-received microstructure to 90 nm at 10 dpa irrespective of the irradiation temperature even till 723 K (Refer Figure S3 for TEM images at

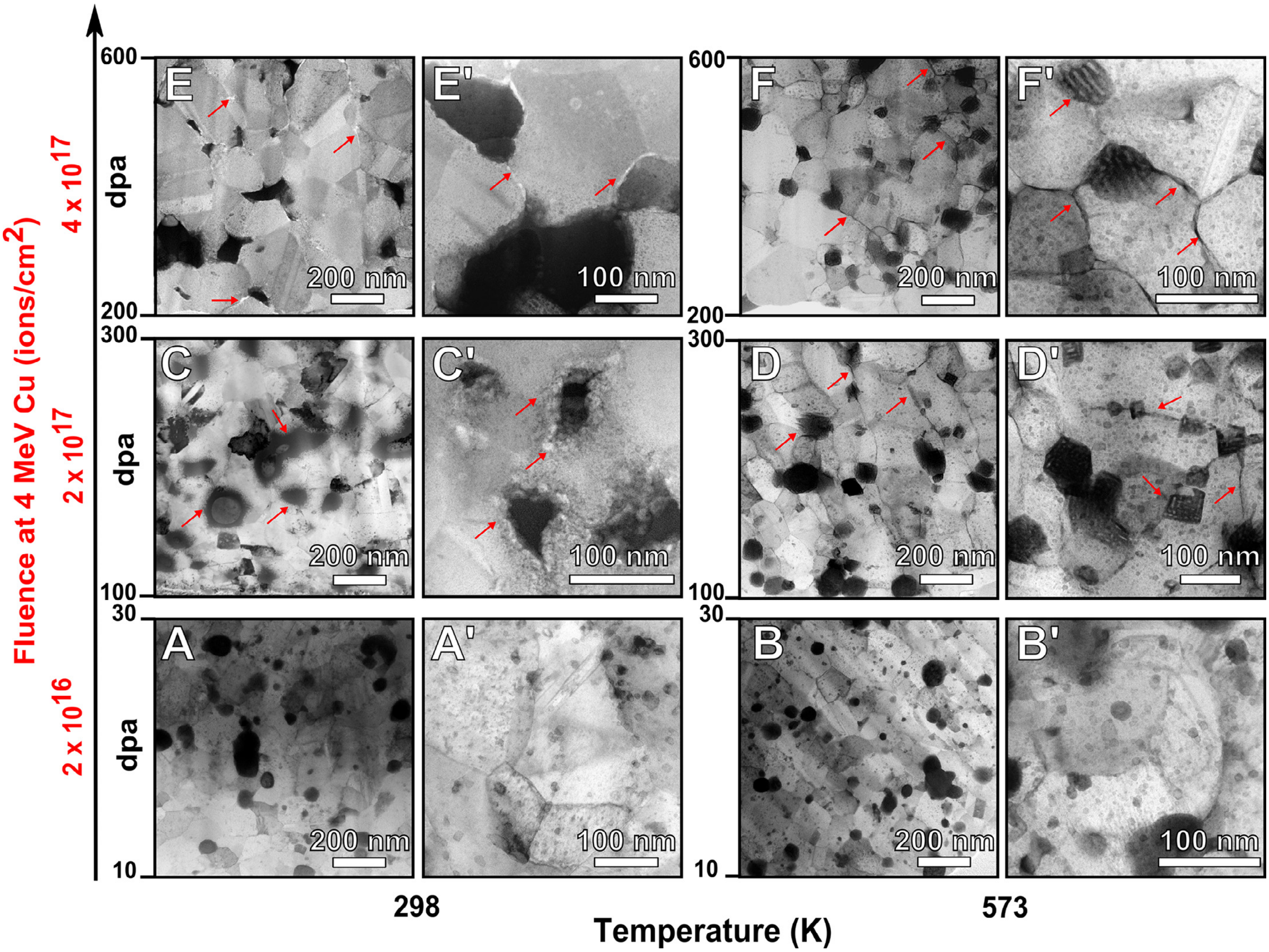

Fig. 5. Cross section bright field STEM images of NC Cu-Ta from the irradiated surface (bottom of each low mag image) to the peak damage region (refer Fig. 2), where the brighter grains are NC Cu and the darker grains/precipitates are Ta, of samples irradiated at **Room temperature** to (A, A') 10 dpa showing the stable microstructure and dislocation activity, (C, C') 100 dpa, highlighting amorphous ring and voids around Ta, respectively (red arrows) and (E, E') 200 dpa revealing voids along GBs and Ta interfaces and larger tantalum dissolution; and **573 K** to (B, B') 10 dpa with fairly unaffected microstructure with minimum grain growth, (D, D') 100 dpa and (F, F') 200 dpa indicating ballistic dissolution of larger Ta phases and their short circuit diffusion along the GBs (red arrows). The corresponding dpa value along the irradiated surface at the bottom and peak damage at the top of low mag images are indicated on their left (A-F). Images (A'-F') are high mag images of the conditions corresponding to (A-F) (For interpretation of the references to color in this figure legend, the reader is referred to the web version of this article.).

723 K). Moreover, the grain size reached an average of 110 and 140 nm for 100 and 200 dpa respectively, with the irradiation temperature having a negligible effect as seen from Fig. 5C–F. The average grain size is thus maintained at nano regime even at such high dose, in comparison to the massive grain growth observed in NC Cu from ~48 to 800 nm at 1 dpa [30] and NC composite of Cu-0.5Al_2O_3 from 180 to 495 nm at 0.9 dpa [43]. In other words, minimal grain growth and microstructural evolution in NC Cu-Ta signals that the stabilized grain boundaries (GBs) act as stable sinks and persist, thereby annihilating irradiation induced defects. In fact, earlier Precession Electron Diffraction (PED) studies on NC Cu-Ta alloy revealed a large fraction of high angle GBs in the material [21], which are naturally more efficient defect sinks [44].

Furthermore, BF TEM and STEM images showed no observed defects post irradiation. Zone axis imaging for the identification of radiation defects was challenging because of the nano-crystallinity of the alloy. HAADF images (which are purely phase contrast) were compared with their corresponding MAADF images (which gives diffraction contrast), to look for defects and differentiate them from Ta clusters. In addition, there was no void swelling observed in samples irradiated to 1 dpa at RT and 10 dpa till 723 K. At 100 dpa and RT, some TEM lamellae showed disordering of the larger Ta interfaces (Fig. 5C); while others showed few voids at the interfaces (Figs. 5C' and S4). Nevertheless, the swelling observed was as low as ~0.2% compared to 0.5% observed in a ODS ferritic alloy MA 957 at 100 dpa under 823 K [45]. At very high dose of 200 dpa at RT, few regions were observed to show continuous voids especially along copper GBs and larger Ta interfaces (Figs. 5E, S4 and S5) but still with no significant swelling. Furthermore, for the irradiation conditions such as 100 and 200 dpa at 573 K (See Fig. 5D&F), voids were extremely difficult to detect using HRTEM images. Overall, this illustrates the remarkable swelling resistance of NC Cu-Ta alloy.

3.3.2. Phase stability

Coherent/semicoherent interfaces of Ta nanoclusters in NC Cu-Ta alloy are key recombination sites for annihilation of vacancies and interstitials due to high as received misfit strain as discussed earlier. Moreover, the as received sink strength (using Eq. (2)) for Ta nanoclusters (average diameter 3.18 nm and density $6.5 \times 10^{23}/m^3$) is $1.3 \times 10^{18}/m^2$, which is two orders of magnitude higher than that for GBs (average grain size 50 nm) with sink

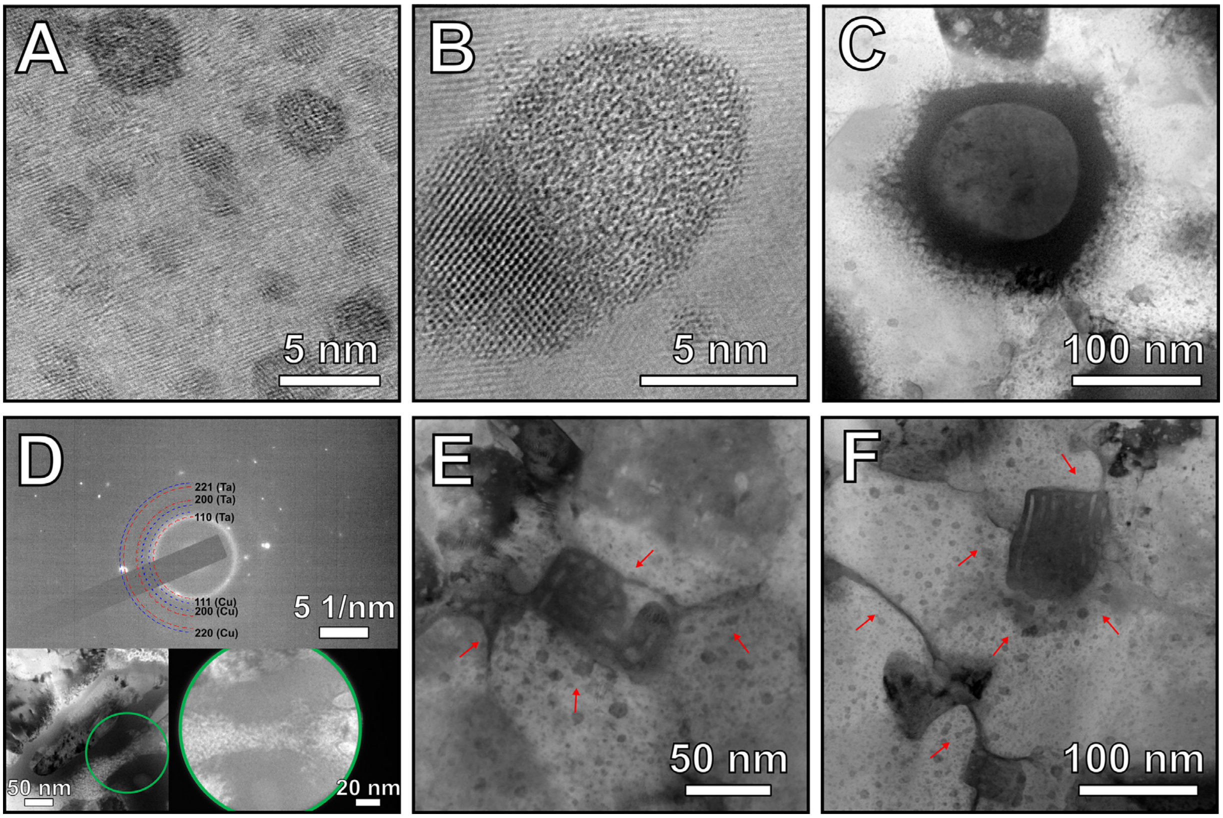

Fig. 6. Tantalum phase post irradiation (A) Ta NCs shown for 200 dpa RT, exhibiting stable core-shell microstructure, (B) HR BF STEM image of a Ta cluster in 10 dpa at 723 K, (C) Amorphous ring in large Ta phase in 100 dpa RT (~400 nm from irradiated surface), (D) SAED of the amorphous region around Ta with the area used to take SAED in 100 dpa at RT (~200 nm from irradiated surface). Standard lattice spacings for Cu (blue) and Ta (red) are overlaid to the SAED pattern. (E-F) STEM BF images from 200 dpa and 573 K of large Ta particle with implanted copper (~300 and 600 nm from irradiated surface, respectively), where Ta is ballistically ejected to lattice and grain boundaries with increased density of Ta nanoclusters in the nearby region indicating precipitation due to dissolution (For interpretation of the references to color in this figure legend, the reader is referred to the web version of this article.).

strength of 6 × $10^{16}/m^2$ in NC Cu-Ta. Further, the dense spacing between these nanoclusters of ~5 nm [19,46] paves the way for overlapping defect denuded zones. Hence, it is paramount to investigate radiation effects on tantalum phase stability including structure, size and density. Several mechanisms have been studied and reviewed on phase stability post-irradiation, which constitutes ballistic dissolution, Ostwald ripening, radiation enhanced diffusion and inverse Ostwald ripening [7,47–49]. For instance, Chen et al. observed shrinkage and dissolution of the oxide particles in 12Cr ODS [50], while Lescoat et al. witnessed growth of oxides in ferritic ODS steels [51]. In NC Cu-Ta alloy, as discussed earlier there are two types of Ta based phases: Ta nanoclusters (≤15 nm) and larger Ta sacrificial particles (>15 nm). Ta nanocluster size distribution determined at different damage levels, from both TEM and atom probe tomography (APT) are in good agreement considering the small sample size, showing that the nanoclusters size does not vary as comparing the as-received condition with the irradiated condition (Fig. S7). Further, the core-shell structure of the nanoclusters with oxygen rich core also seems to be maintained post irradiation as seen in Fig. 6(A and B).

However, the larger Ta sacrificial particles developed amorphous ring (Fig. 6C) due to ballistic mixing along the interface in room temperature irradiations where diffusion is sluggish, and at damage levels > ~20 dpa. This is confirmed using a selected area diffraction pattern (Fig. 6D) on the region surrounding the tantalum particle irradiated to 100 dpa at RT, which showed an obvious diffused ring at Ta (110) lattice spacing position (and a mild one at Ta (221)). The halo size increased and became prominent with dose since ballistic mixing across the interface is proportional to the fluence. Excessive accumulation of defects and chemical disordering at the incoherent Ta interface due to the dense cascades has increased the free energy of the system enabling amorphization [52]. At 100 and 200 dpa and RT, the larger tantalum particles were also observed to undergo short-circuit diffusion along copper grain boundaries with minimum/no amorphization observed at 200 dpa and RT. The observed disordering (mixing) could thus, be a precursor/transient state for dissolution of the tantalum particles. Computational studies have shown similar amorphization due to shear induced chemical mixing at the precipitate-matrix interfaces of Cu-Nb (4 at.%) and Cu-V (8 at.%), which increased linearly with particle radius [53]. It was also reported that semi-coherent interfaces were more stable and resistant to amorphization. Moreover, Sauvage et.al reported that the amorphous interface they observed post wire drawing in Cu-Nb were associated with very fine precipitates due to mixing of Cu and Nb [54]. Alternatively, in the corresponding 573 K irradiations (Fig. 6E and F), where diffusion is significant for thermal reordering, larger Ta sacrificial particles did not exhibit any disordering. Existence of critical amorphization temperature has been confirmed in many previous studies. For instance, Ribis et al. [55] showed amorphization of ODS particles at RT while regaining crystallinity at 773 K, and Lescoat et al. observed amorphization of oxide particles (>50 nm) in ODS steels with existence of critical amorphization temperature [51]. Moreover, mixing/dissolution of solute in the solvent lattice in “driven” alloys is a result of competition between forced mixing (ballistic effects) and thermal diffusion, where the forc-

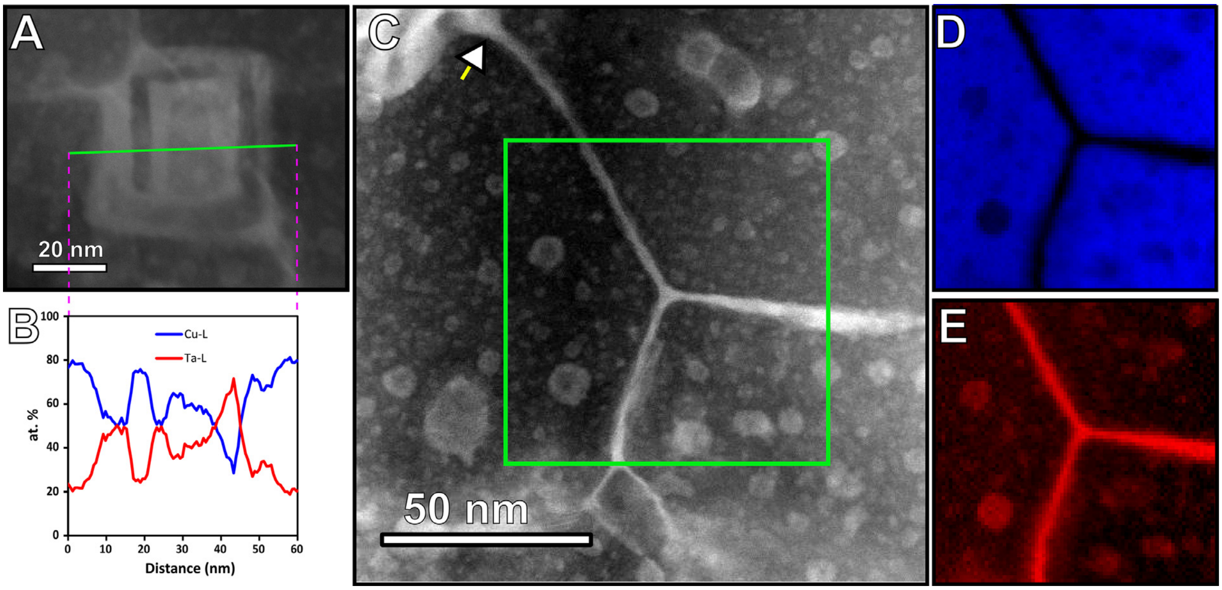

Fig. 7. Elemental analysis of Ta segregation. (A) HAADF image of a Ta particle with patterns of implanted copper where tantalum is ballistically ejected, (B) Line scan of the highlighted area in A showing increase in copper and decrease in tantalum concentration in the patterned region within the tantalum particle indicating knocking out of tantalum by implanted copper, (C) HAADF image of a Cu10at%Ta tested at 200 dpa and 573 K showing a dissolving Ta particle preferentially diffusing along a GB, (D) EELS Cu-K map in blue, of the region highlighted in green in C, showing the grain boundary region devoid of copper. (E) Ta-L map in red, of the region highlighted in green in C showing diffusion of tantalum along grain boundaries (For interpretation of the references to color in this figure legend, the reader is referred to the web version of this article.).

ing parameter 'γ' (given by $\gamma = \Gamma_b / \Gamma_t$ [56]), decreases with temperature.

Additionally, in high dose cases ($\geq$ 100 dpa) at 573 K, the large Ta particles developed a patterned structure with implanted Cu atoms as observed in Fig. 6(E and F) due to the energetic recoils. Energy dispersive spectroscopy (EDS) line scans (Fig. 7A and B) along the pattern, confirmed an increased concentration of Cu and a depletion of Ta in patterned regions within the Ta particles, indicating knock out of Ta atoms by implanted Cu atoms. As Cu and Ta are phase separating (positive enthalpy of mixing), at elevated temperatures the implantation of Cu leads to a re-arrangement and the development of a spinodal microstructure through short-range diffusion. In addition to the Cu ion implantation, the large Ta particles has undergone ballistic dissolution within the surrounding microstructure. (Fig. 2(E, E', F, and F')). The Nelson, Hudson, and Mazey (NHM) model describes precipitate dissolution at a displacement rate k, due to scattering of atoms from precipitates of radius r_p, number density ρ, and solute concentration C_p, through the following equation [57,58],

$$\frac{dr_p}{dt} = -yk + \frac{3DC}{4\pi r_p C_p} - r_p^2 D\rho \tag{3}$$

where C is the total solute concentration, D is the solute diffusion coefficient, and y is a constant representing thickness of atom layers scattered from the precipitate per dpa. Considering sputtering of tantalum atoms, the NHM model suggested a y-value of 10^4 cm/dpa, which was utilized for the calculation. Using the above equation for a Ta particle of average radius 25 nm (from TEM), a negative rate of change was calculated (i.e., $dr/dt < 0$), indicating dissolution of large Ta particles.

Dissolution of the larger particles led to a local enrichment of Ta solute in the nearby (surrounding) lattice regions. However, as the material was irradiated further (Radiation enhanced diffusion) and the temperature increased (γ reduces), these supersaturated Ta regions began to form nanoclusters (Fig. 6D–F), a process which requires diffusion-controlled redistribution of Ta. We emphasize that this process under non-irradiated conditions is only possible along GBs, which offer faster diffusion pathways; since it cannot occur in the Cu lattice, where Ta diffusion is extremely slow even near the melting point. Moreover, under irradiation, the tendency to form Ta nanoclusters may be similar in atomic origin to the formation of stable nano emulsions found in liquid Cu–Ta alloys, stabilized by a negative and strongly curvature-dependent tension of the Cu-Ta interfaces [59], which limit any coarsening due to balance between the deterministic reaction and very slow stochastic lattice diffusion force. Such an analogy is supported by the high degree of intense cascading effects, which saturates the structure with point defects. This disordered state offers a "liquid-like" environment for nanocluster formation and provides a path way for local short-circuit diffusion for Ta redistribution within the lattice. Analogous to the stabilized nano-emulsions of Cu-Ta reported by Frolov et al. [59], these newly generated Ta based clusters also resist coarsening despite the intense irradiation and temperature exposure, retaining an average diameter $<$ 10 nm.

Furthermore, in addition to Ta saturation within the lattice, electron energy loss spectroscopy (EELS) analysis along a GB triple junction (Fig. 7C–E) in a 200 dpa 573 K sample showed that these regions were also being enriched with Ta solute from nearby large Ta particles, which were undergoing ballistic dissolution. Marwick had speculated such segregation of slow diffusing solute elements (inverse Kirkendall effect) to the sinks due to difference in vacancy diffusion coefficients of the alloy constituents [60]. The Ta solute atoms diffusing along the intergranular regions are eventually precipitated as nanoclusters due to supersaturation of Ta solute, resulting in a high cluster density within these regions as well (Fig. 7C). Russell had predicted this behavior of dissolution and re-precipitation of second phase particles due to recoils, where the dissolved large particle will be replaced with finer particles with continued irradiation [61]. Likewise, Chen et al. and Lu et al. have reported dissolution of larger particles and precipitation of fine dispersoids in ODS alloys after high dose self-ion and helium pre-implanted self-ion irradiations respectively [50,62]. While Certain et al. observed dissolution of nanoclusters in 14YWT at low temperatures while being stable at high temperatures, due to diffusion

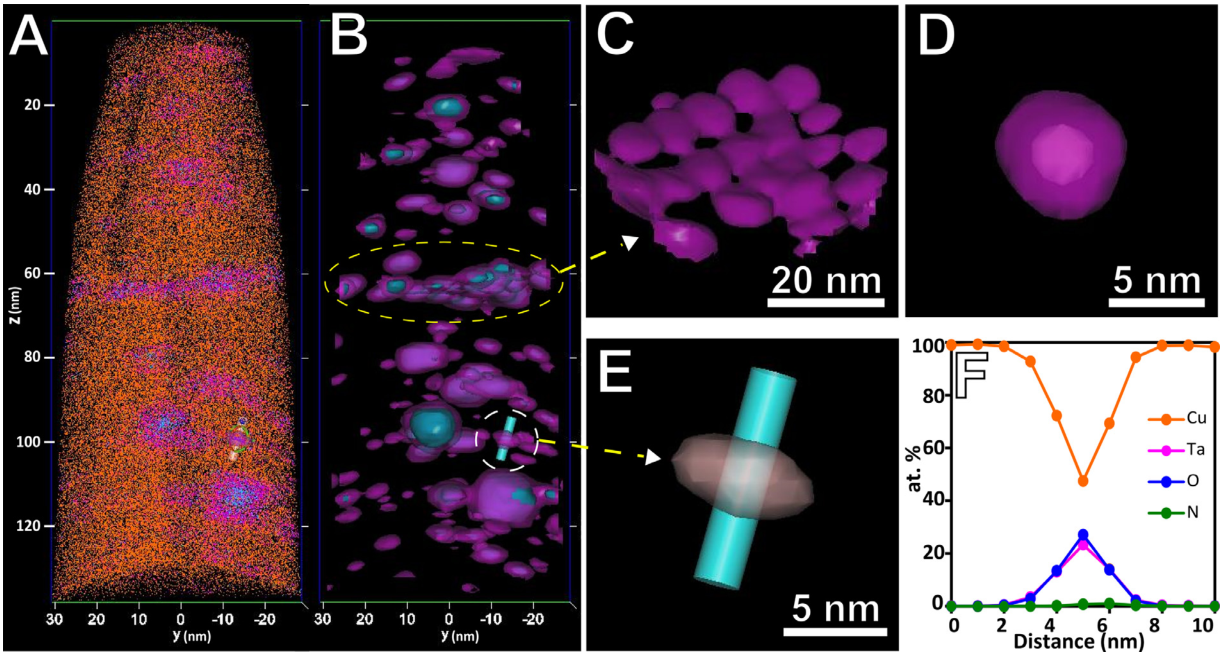

Fig. 8. (A) Atom distribution map of APT specimen prepared from the irradiated surface (to a depth of 140 nm) of 100 dpa irradiation at 573K, where Cu is shown in orange, Ta in purple and O in blue; (B) Ta and O delineated with 5 at. % Ta iso-concentration surface in purple with 21 at. % O iso-concentration surface in blue; (C) GB circled in (B) showing continuous Ta interface along the grain boundary; (D) 5 at.% Ta iso-concentration surface surrounding a 21% O iso-concentration surface, representing a core-shell structured Ta particle; (E) A cylinder passing through the Ta particle circled in (B); (F) 1D concentration profile generated from the cylinder shown in (E), showing a representative chemical composition for the Ta particles (For interpretation of the references to color in this figure legend, the reader is referred to the web version of this article.).

of dissolved solute back to the parent cluster, with no new precipitation [63]. Atom probe analysis in Fig. 8 provided additional proof of short-circuit diffusion in the form of compositional modulation along the GBs due to decrease in total surface energy of the Ta phase, which is the precursor to cluster formation (Fig. 8C). Correspondingly, the role of this short circuit diffusion of Ta at mobile GBs has been analyzed previously and has been shown to leave behind residual clusters within the lattice; thereby allowing a second mechanism to increase sink concentration (Fig. 8D and E) [64].

Furthermore, it is interesting to note that the ascribed microstructural evolution process observed from irradiating this matter at elevated temperatures is similar to the mechanical dissolution experienced during the initial synthesis of the material via high energy mechanical alloying. That is, synthesis through ball milling also introduces a high density of non-equilibrium linear and point defects, as well as the creation of super saturated solid solutions. This combination leads to enriched Ta regions which evolve through phase separation and short-circuit diffusion at elevated temperatures to yield increased cluster densities and homogenous dispersions. This microstructure can then be restored to the initial state of dissolution through application of additional mechanical alloying and the generation of new defects in a repetitive manner yielding the final-end state each time. This idea of rejuvenation through mechanical alloying is analogous to the irradiation process where larger particles can be re-dissolved and smaller particles precipitated and coarsened, which is typically a dynamic balance between the ballistic mixing effects and thermal diffusion induced decomposition in a driven system. Interestingly, even with the application of radiation, the rate of coarsening of the small clusters ($<$ 10nm) is still extremely sluggish as noted in TEM images, Fig. 6A and S7. This is only possible through the radiation induced generation and decomposition of metastable solid solutions, in a system with a positive enthalpy of mixing between the respective constituents. Such an analogy will hold true as long as the system remains free of minor constituents that would form ordered or ceramic phases, and the precipitating phase is in surplus to those as in the case of Ta in Cu. Various computational and experimental studies have exploited the role of compositional self-organization (steady state/patterning) in binary alloys with positive heat of mixing, observed at a specific range of temperature and shearing rates, in maintaining refined microstructure during high temperature irradiations or ball milling for long durations [65–67]. Further, Chee et. al. reported the maximum temperature of patterning regime (temperature for microscopic coarsening, T_{max}) for various Cu based alloys, where systems with high positive heat of mixing like Cu-Nb and Cu-V experienced a higher T_{max} ($>$773 K) [68]. Additionally, high density of sinks have been predicted to have a positive role in stabilizing irradiation induced patterning [69]. No evident coarsening of clusters in NC Cu-Ta even at 723 K could indicate a large patterning regime due to high sink density and positive enthalpy of mixing, which is an area to be explored further in detail.

Altogether, the response of NC Cu-Ta at each damage level and temperature, with respect to grain growth and phase changes is depicted in Fig. 9, where initial grain growth observed till 10 dpa (possibly due to dissolution of clusters), gets saturated at 100 dpa and beyond due to precipitation of more new clusters pinning the grain boundaries. Ballistic mixing at RT in the Ta interface induces dissolution at doses $\geq$ 100 dpa. As the dose and temperature increases, short circuit diffusion of Ta occurs through grain boundaries and phase separation gains dominance, thereby precipitating more smaller clusters from the supersaturated regions and replenishing the sink density. Therefore, designing alloys employing positively phase separating elements in their makeup with sacrificial phases, plays a key role in developing radiation tolerance whereby the number of available interfaces acting as potent and stable sinks is increased significantly as demonstrated here. Thus, this paves a pathway for development of cutting-edge structural materials for extreme radiation applications, such as space exploration and next generation nuclear reactors.

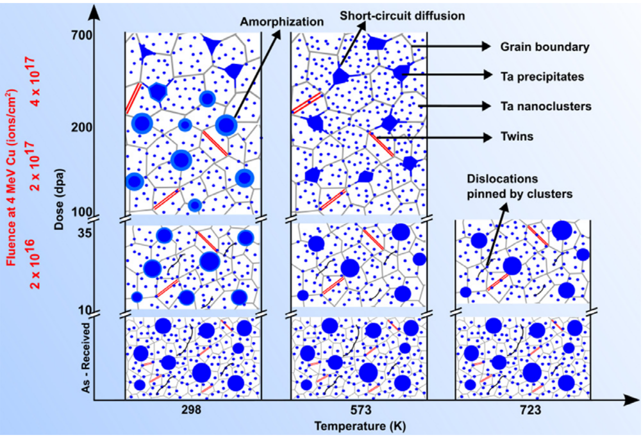

Fig. 9. Radiation response mechanism in nanocrystalline Cu-Ta. Condensed microstructural response and phase changes in NC Cu-Ta at different irradiation conditions characterized in this study. Copper matrix is represented in white and the blue blobs represent tantalum (For interpretation of the references to color in this figure legend, the reader is referred to the web version of this article.).

4. Conclusions

In this work, an exceptional radiation tolerance along with microstructural stability in an immiscible NC Cu-10at.% Ta is experimentally demonstrated and the following important conclusions can be drawn:

- Very minimum radiation hardening at room temperature and 573 K, up to 100 dpa, as compared to many advanced structural materials from literature
- Marginal increase in grain size from 50 nm in the as received condition to around 110 nm and 140 nm at high doses of 100 and 200 dpa respectively, with negligible effect of irradiation temperatures on the grain size
- Remarkable swelling resistance as seen from low swelling observed only at 100 dpa (0.2 %) and 200 dpa at room temperature, while no voids observed at the corresponding 573 K irradiations and other lower doses
- The larger Ta phases disintegrate and segregate along copper grain boundaries and eventually re-precipitates as Ta rich nanoclusters at high doses ($\geq$ 100 dpa), with no apparent coarsening of the nanoclusters

The key aspects for the observed radiation response are, the stability of nanoclusters which is partly attributed to emulsion-like behavior due to the phase separating nature of the material system; and their replenishment by the dissolution of sacrificial phase. This enables restoring the microstructure to initial state with additional doses in a repetitive manner, evolving a self-healing mechanism in the material while maintaining superior mechanical strength and temperature properties.

Declaration of Competing Interest

The authors declare that they have no known competing financial interests or personal relationships that could have appeared to influence the work reported in this paper.

Acknowledgment

Ion irradiation was performed at the Center for Integrated Nanotechnologies (CINT), an Office of Science User Facility operated for the U.S. Department of Energy (DOE) Office of Science. Los Alamos National Laboratory, an affirmative action equal opportunity employer, is managed by Triad National Security, LLC for the U.S. Department of Energy's NNSA, under contract 89233218CNA000001. S.S., C.K. and K. N. S. acknowledge the use of facilities within the LeRoy Eyring Center for Solid State Science at Arizona State University and Atom probe facility at CAMECA Inc. This work was supported by US Army Research Laboratory under contract W911NF-15-2-0038 and the National Science Foundation No. 1663287. K.A.D acknowledges A.J Roberts, M. Gallagher, and T. Luckenbaugh for synthesis of the Cu-Ta powder.

Supplementary materials

Supplementary material associated with this article can be found, in the online version, at doi:10.1016/j.actamat.2020.05.061.

References

[1] S.J. Zinkle, G.S. Was, Materials challenges in nuclear energy, Acta Mater 61 (2013) 735–758, doi:10.1016/j.actamat.2012.11.004.
[2] K.L. Murty, I. Charit, Structural materials for Gen-IV nuclear reactors: Challenges and opportunities, J. Nucl. Mater. 383 (2008) 189–195, doi:10.1016/j.jnucmat.2008.08.044.
[3] S.J. Zinkle, J.T. Busby, Structural materials for fission & fusion energy, Mater. Today. 12 (2009) 12–19.
[4] V.V. Sagaradze, V.I. Shalaev, V.L. Arbuzov, B.N. Goshchitskii, Y. Tian, W. Qun, S. Jiguang, Radiation resistance and thermal creep of ODS ferritic steels, J. Nucl. Mater. 295 (2001) 265–272, doi:10.1016/S0022-3115(01)00511-6.
[5] A. Alamo, J.L. Bertin, V.K. Shamardin, P. Wident, Mechanical properties of 9Cr martensitic steels and ODS-FeCr alloys after neutron irradiation at 325°C up to 42dpa, J. Nucl. Mater. 367–370 (2007) 54–59, doi:10.1016/j.jnucmat.2007.03.166.
[6] A. Alamo, M. Horsten, X. Averty, E.. Materna-Morris, M. Rieth, J. Brachet, Mechanical behavior of reduced-activation and conventional martensitic steels after neutron irradiation in the range 250–450°C, J. Nucl. Mater. 283–287 (2000) 353–357, doi:10.1016/S0022-3115(00)00076-3.
[7] J.P. Wharry, M.J. Swenson, K.H. Yano, A review of the irradiation evolution of dispersed oxide nanoparticles in the b.c.c. Fe-Cr system: Current understanding and future directions, J. Nucl. Mater. 486 (2017) 11–20, doi:10.1016/j.jnucmat.2017.01.009.
[8] W. Han, M.J. Demkowicz, N.A. Mara, E. Fu, S. Sinha, A.D. Rollett, Y. Wang, J.S. Carpenter, I.J. Beyerlein, A. Misra, Design of radiation tolerant materials via interface engineering, Adv. Mater. 25 (2013) 6975–6979, doi:10.1002/adma.201303400.
[9] M.J. Demkowicz, R.G. Hoagland, J.P. Hirth, Interface structure and radiation damage resistance in Cu-Nb multilayer nanocomposites, Phys. Rev. Lett. 100 (2008) 136102, doi:10.1103/PhysRevLett.100.136102.
[10] A. Misra, M.J. Demkowicz, X. Zhang, R.G. Hoagland, The radiation damage tolerance of ultra-high strength nanolayered composites, JOM 59 (2007) 62–65, doi:10.1007/s11837-007-0120-6.
[11] G.M. Cheng, W.Z. Xu, Y.Q. Wang, A. Misra, Y.T. Zhu, Grain size effect on radiation tolerance of nanocrystalline Mo, Scr. Mater. 123 (2016) 90–94, doi:10.1016/j.scriptamat.2016.06.007.
[12] I.J. Beyerlein, A. Caro, M.J. Demkowicz, N.A. Mara, A. Misra, B.P. Uberuaga, Radiation damage tolerant nanomaterials, Mater. Today. 16 (2013) 443–449, doi:10.1016/j.mattod.2013.10.019.
[13] S. Wurster, R. Pippan, Nanostructured metals under irradiation, Scr. Mater. 60 (2009) 1083–1087, doi:10.1016/j.scriptamat.2009.01.011.
[14] G.S. Was, Fundamentals of Radiation Materials Science: Metals and Alloys, 2nd ed., Springer-Verlag, New York, 2017 https://www.springer.com/gp/book/9781493934362.
[15] E. Ma, Alloys created between immiscible elements, Prog. Mater. Sci. 50 (2005) 413–509, doi:10.1016/j.pmatsci.2004.07.001.
[16] L.C. Wei, R.S. Averback, Phase evolution during ion-beam mixing of Ag–Cu, J. Appl. Phys. 81 (1997) 613–623, doi:10.1063/1.364202.
[17] R.K. Koju, K.A. Darling, K.N. Solanki, Y. Mishin, Atomistic modeling of capillary-driven grain boundary motion in Cu-Ta alloys, Acta Mater 148 (2018) 311–319, doi:10.1016/j.actamat.2018.01.027.
[18] K.A. Darling, M. Rajagopalan, M. Komarasamy, M.A. Bhatia, B.C. Hornbuckle, R.S. Mishra, K.N. Solanki, Extreme creep resistance in a microstructurally stable nanocrystalline alloy, Nature 537 (2016) 378–381, doi:10.1038/nature19313.
[19] S.A. Turnage, M. Rajagopalan, K.A. Darling, P. Garg, C. Kale, B.G. Bazehhour, I. Adlakha, B.C. Hornbuckle, C.L. Williams, P. Peralta, K.N. Solanki, Anomalous mechanical behavior of nanocrystalline binary alloys under extreme conditions, Nat. Commun. 9 (2018) 2699, doi:10.1038/s41467-018-05027-5.
[20] M. Rajagopalan, K.A. Darling, C. Kale, S.A. Turnage, R.K. Koju, B.C. Hornbuckle, Y. Mishin, K.N. Solanki, Nanotechnology enabled design of a structural material with extreme strength as well as thermal and electrical properties, Mater. Today 31 (2019) 10–20, doi:10.1016/j.mattod.2019.09.024.
[21] M. Rajagopalan, K. Darling, S. Turnage, R.K. Koju, B. Hornbuckle, Y. Mishin, K.N. Solanki, Microstructural evolution in a nanocrystalline Cu-Ta alloy: A combined in-situ TEM and atomistic study, Mater. Des. 113 (2017) 178–185, doi:10.1016/j.matdes.2016.10.020.

[22] M. Bhatia, M. Rajagopalan, K. Darling, M. Tschopp, K. Solanki, The role of Ta on twinnability in nanocrystalline Cu–Ta alloys, Mater. Res. Lett. 5 (2017) 48–54.

[23] R.E. Stoller, M.B. Toloczko, G.S. Was, A.G. Certain, S. Dwaraknath, F.A. Garner, On the use of SRIM for computing radiation damage exposure, Nucl. Instrum. Methods Phys. Res. Sect. B Beam Interact. Mater. At. 310 (2013) 75–80, doi:10.1016/j.nimb.2013.05.008.

[24] Standard Practice for Neutron Radiation Damage Simulation by Charged-Particle Irradiation, 96.

[25] P. Hosemann, D. Kiener, Y. Wang, S.A. Maloy, Issues to consider using nano indentation on shallow ion beam irradiated materials, J. Nucl. Mater. 425 (2012) 136–139, doi:10.1016/j.jnucmat.2011.11.070.

[26] M.B. Toloczko, F.A. Garner, V.N. Voyevodin, V.V. Bryk, O.V. Borodin, V.V. Mel'nychenko, A.S. Kalchenko, Ion-induced swelling of ODS ferritic alloy MA957 tubing to 500 DPA, J. Nucl. Mater. 453 (2014) 323–333, doi:10.1016/j.jnucmat.2014.06.011.

[27] S.I. Golubov, A.V. Barashev, R.E. Stoller, 1.13 - Radiation Damage Theory, in: R.J.M. Konings (Ed.), Comprehensive Nuclear Materials, Elsevier, Oxford, 2012, pp. 357–391, doi:10.1016/B978-0-08-056033-5.00029-X.

[28] B.C. Hornbuckle, T. Rojhirunsakool, M. Rajagopalan, T. Alam, G.P. Purja Pun, R. Banerjee, K.N. Solanki, Y. Mishin, L.J. Kecskes, K.A. Darling, Effect of Ta Solute Concentration on the Microstructural Evolution in Immiscible Cu-Ta Alloys, JOM 67 (2015) 2802–2809, doi:10.1007/s11837-015-1643-x.

[29] A.C. Fischer-Cripps, Nanoindentation Testing, in: A.C. Fischer-Cripps (Ed.), Nanoindentation, Springer New York, New York, NY, 2011, pp. 21–37, doi:10.1007/978-1-4419-9872-9_2.

[30] W. Mohamed, B. Miller, D. Porter, K. Murty, The role of grain size on neutron irradiation response of nanocrystalline copper, Materials 9 (2016) 144, doi:10.3390/ma9030144.

[31] E.G. Fu, H. Wang, J. Carter, L. Shao, Y.Q. Wang, X. Zhang, Fluence-dependent radiation damage in helium (He) ion-irradiated Cu/V multilayers, Philos. Mag. 93 (2013) 883–898, doi:10.1080/14786435.2012.735773.

[32] D.L. Krumwiede, T. Yamamoto, T.A. Saleh, S.A. Maloy, G.R. Odette, P. Hosemann, Direct comparison of nanoindentation and tensile test results on reactor-irradiated materials, J. Nucl. Mater. 504 (2018) 135–143, doi:10.1016/j.jnucmat.2018.03.021.

[33] Z. Jiao, G.S. Was, The role of irradiated microstructure in the localized deformation of austenitic stainless steels, J. Nucl. Mater. 407 (2010) 34–43, doi:10.1016/j.jnucmat.2010.07.006.

[34] T. Zhang, C. Vieh, K. Wang, Y. Dai, Irradiation-induced evolution of mechanical properties and microstructure of Eurofer 97, J. Nucl. Mater. 450 (2014) 48–53, doi:10.1016/j.jnucmat.2013.12.007.

[35] A. Lupinacci, K. Chen, Y. Li, M. Kunz, Z. Jiao, G.S. Was, M.D. Abad, A.M. Minor, P. Hosemann, Characterization of ion beam irradiated 304 stainless steel utilizing nanoindentation and Laue microdiffraction, J. Nucl. Mater. 458 (2015) 70–76, doi:10.1016/j.jnucmat.2014.11.050.

[36] L. Fave, M.A. Pouchon, M. Döbeli, M. Schulte-Borchers, A. Kimura, Helium ion irradiation induced swelling and hardening in commercial and experimental ODS steels, J. Nucl. Mater. 445 (2014) 235–240, doi:10.1016/j.jnucmat.2013.11.004.

[37] C. Liu, C. Yu, N. Hashimoto, S. Ohnuki, M. Ando, K. Shiba, S. Jitsukawa, Microstructure and micro-hardness of ODS steels after ion irradiation, J. Nucl. Mater. 417 (2011) 270–273, doi:10.1016/j.jnucmat.2011.01.067.

[38] B. Duan, C. Heintze, F. Bergner, A. Ulbricht, S. Akhmadaliev, E. Oñorbe, Y. de Carlan, T. Wang, The effect of the initial microstructure in terms of sink strength on the ion-irradiation-induced hardening of ODS alloys studied by nanoindentation, J. Nucl. Mater. 495 (2017) 118–127, doi:10.1016/j.jnucmat.2017.08.014.

[39] E. Aydogan, J.S. Weaver, S.A. Maloy, O. El-Atwani, Y.Q. Wang, N.A. Mara, Microstructure and mechanical properties of FeCrAl alloys under heavy ion irradiations, J, Nucl. Mater. 503 (2018) 250–262, doi:10.1016/j.jnucmat.2018.03.002.

[40] F. Lu, M. Huang, F. Yaqoob, M. Lang, F. Namavar, C. Trautmann, H. Sun, R.C. Ewing, J. Lian, Displacive radiation-induced structural contraction in nanocrystalline ZrN, Appl. Phys. Lett. 101 (2012) 041904, doi:10.1063/1.4738772.

[41] X. Zhang, E.G. Fu, A. Misra, M.J. Demkowicz, Interface-enabled defect reduction in He ion irradiated metallic multilayers, JOM 62 (2010) 75–78, doi:10.1007/s11837-010-0185-5.

[42] T. Rojhirunsakool, K.A. Darling, M.A. Tschopp, G.P. Purja Pun, Y. Mishin, R. Banerjee, L.J. Kecskes, Structure and thermal decomposition of a nanocrystalline mechanically alloyed supersaturated Cu–Ta solid solution, MRS Commun 5 (2015) 333–339, doi:10.1557/mrc.2015.34.

[43] X. Zhang, K. Hattar, Y. Chen, L. Shao, J. Li, C. Sun, K. Yu, N. Li, M.L. Taheri, H. Wang, J. Wang, M. Nastasi, Radiation damage in nanostructured materials, Prog. Mater. Sci. 96 (2018) 217–321, doi:10.1016/j.pmatsci.2018.03.002.

[44] M.A. Tschopp, K.N. Solanki, F. Gao, X. Sun, M.A. Khaleel, M.F. Horstemeyer, Probing grain boundary sink strength at the nanoscale: Energetics and length scales of vacancy and interstitial absorption by grain boundaries in α-Fe, Phys. Rev. B. 85 (2012) 064108, doi:10.1103/PhysRevB.85.064108.

[45] M.. Toloczko, D.. Gelles, F.. Garner, R.. Kurtz, K. Abe, Irradiation creep and swelling from 400 to 600°C of the oxide dispersion strengthened ferritic alloy MA957, J. Nucl. Mater. 329–333 (2004) 352–355, doi:10.1016/j.jnucmat.2004.04.296.

[46] C. Kale, S. Turnage, P. Garg, I. Adlakha, S. Srinivasan, B.C. Hornbuckle, K. Darling, K.N. Solanki, Thermo-mechanical strengthening mechanisms in a stable nanocrystalline binary alloy – A combined experimental and modeling study, Mater. Des. 163 (2019) 107551, doi:10.1016/j.matdes.2018.107551.

[47] T.R. Allen, J. Gan, J.I. Cole, M.K. Miller, J.T. Busby, S. Shutthanandan, S. Thevuthasan, Radiation response of a 9 chromium oxide dispersion strengthened steel to heavy ion irradiation, J. Nucl. Mater. 375 (2008) 26–37, doi:10.1016/j.jnucmat.2007.11.001.

[48] K.C. Russell, Phase stability under irradiation, Prog. Mater. Sci. (n.d.) 206.

[49] M.J. Swenson, J.P. Wharry, Nanocluster irradiation evolution in Fe-9%Cr ODS and ferritic-martensitic alloys, J. Nucl. Mater. 496 (2017) 24–40, doi:10.1016/j.jnucmat.2017.08.045.

[50] T. Chen, E. Aydogan, J.G. Gigax, D. Chen, J. Wang, X. Wang, S. Ukai, F.A. Garner, L. Shao, Microstructural changes and void swelling of a 12Cr ODS ferritic-martensitic alloy after high-dpa self-ion irradiation, J. Nucl. Mater. 467 (2015) 42–49, doi:10.1016/j.jnucmat.2015.09.016.

[51] M.-L. Lescoat, I. Monnet, J. Ribis, P. Dubuisson, Y. de Carlan, J.-M. Costantini, J. Malaplate, Amorphization of oxides in ODS materials under low and high energy ion irradiations, J. Nucl. Mater. 417 (2011) 266–269, doi:10.1016/j.jnucmat.2011.01.065.

[52] A.T. Motta, C. Lemaignan, A ballistic mixing model for the amorphization of precipitates in Zircaloy under neutron irradiation, J. Nucl. Mater. 195 (1992) 277–285, doi:10.1016/0022-3115(92)90519-Q.

[53] Y. Ashkenazy, N.Q. Vo, D. Schwen, R.S. Averback, P. Bellon, Shear induced chemical mixing in heterogeneous systems, Acta Mater 60 (2012) 984–993, doi:10.1016/j.actamat.2011.11.014.

[54] X. Sauvage, L. Renaud, B. Deconihout, D. Blavette, D.H. Ping, K. Hono, Solid state amorphization in cold drawn Cu/Nb wires, Acta Mater 49 (2001) 389–394, doi:10.1016/S1359-6454(00)00338-4.

[55] J. Ribis, M.-L. Lescoat, Y. de Carlan, J.-M. Costantini, I. Monnet, T. Cozzika, F. Delabrouille, J. Malaplate, Stability of nano-oxides upon heavy ion irradiation of an ODS material, J. Nucl. Mater. 417 (2011) 262–265, doi:10.1016/j.jnucmat.2010.12.068.

[56] K. Uenishi, K.F. Kobayashi, S. Nasu, H. Hatano, K.N. Ishihara, P.H. Shingu, Mechanical alloying in the Fe-Cu system, Mech. Alloy. Fe-Cu Syst. 83 (1992) 132–135.

[57] R.S. Nelson, J.A. Hudson, D.J. Mazey, The stability of precipitates in an irradiation environment, J. Nucl. Mater. 44 (1972) 318–330, doi:10.1016/0022-3115(72)90043-8.

[58] P. Wilkes, Phase stability under irradiation — a review of theory and experiment, J. Nucl. Mater. 83 (1979) 166–175, doi:10.1016/0022-3115(79)90602-0.

[59] T. Frolov, Y. Mishin, Stable Nanocolloidal Structures in Metallic Systems, Phys. Rev. Lett. 104 (2010) 055701, doi:10.1103/PhysRevLett.104.055701.

[60] A.D. Marwick, Segregation in irradiated alloys: The inverse Kirkendall effect and the effect of constitution on void swelling, J. Phys. F Met. Phys. 8 (1978) 1849–1861, doi:10.1088/0305-4608/8/9/008.

[61] K.C. Russell, Phase instability under cascade damage irradiation, J. Nucl. Mater 206 (1993) 129–138, doi:10.1016/0022-3115(93)90120-N.

[62] C. Lu, Z. Lu, X. Wang, R. Xie, Z. Li, M. Higgins, C. Liu, F. Gao, L. Wang, Enhanced Radiation-tolerant Oxide Dispersion Strengthened Steel and its Microstructure Evolution under Helium-implantation and Heavy-ion Irradiation, Sci. Rep. 7 (2017) 40343, doi:10.1038/srep40343.

[63] A. Certain, S. Kuchibhatla, V. Shutthanandan, D.T. Hoelzer, T.R. Allen, Radiation stability of nanoclusters in nano-structured oxide dispersion strengthened (ODS) steels, J. Nucl. Mater. 434 (2013) 311–321, doi:10.1016/j.jnucmat.2012.11.021.

[64] R.K. Koju, K.A. Darling, L.J. Kecskes, Y. Mishin, Zener pinning of grain boundaries and structural stability of immiscible alloys, JOM 68 (2016) 1596–1604, doi:10.1007/s11837-016-1899-9.

[65] P. Pochet, P. Bellon, L. Chaffron, G. Martin, Phase transformations under ball milling: theory versus experiment, Mater. Sci. Forum. 225–227 (1996) 207–216, doi:10.4028/www.scientific.net/MSF.225-227.207.

[66] R.A. Enrique, P. Bellon, Compositional patterning in systems driven by competing dynamics of different length scale, Phys. Rev. Lett. 84 (2000) 2885–2888, doi:10.1103/PhysRevLett.84.2885.

[67] R.A. Enrique, P. Bellon, Compositional patterning in immiscible alloys driven by irradiation, Phys. Rev. B. 63 (2001) 134111, doi:10.1103/PhysRevB.63.134111.

[68] S.W. Chee, B. Stumphy, N.Q. Vo, R.S. Averback, P. Bellon, Dynamic self-organization in Cu alloys under ion irradiation, Acta Mater 58 (2010) 4088–4099, doi:10.1016/j.actamat.2010.03.039.

[69] S. Shu, P. Bellon, R.S. Averback, Role of point-defect sinks on irradiation-induced compositional patterning in model binary alloys, Phys. Rev. B. 91 (2015) 214107, doi:10.1103/PhysRevB.91.214107.